Design of Chalmers new low-pressure compressor test facility for low-speed testing of cryo-engine applications

Design of Chalmers new low-pressure compressor test facility for low-speed testing of cryo-engine applications

I. Jonsson, G. Debarshee, C. Xisto, T. Grönstedt

Division of Fluid Dynamics, M2, Chalmers University of Technology, Gothenburg, Sweden
Correspondence to: isak.jonsson@chalmers.se

ABSTRACT

As a part of the ongoing Horizon 2020 ENABLEH2 project, a new low-speed compressor test facility is being constructed at the Chalmers University Laboratory of Fluids and Thermal Sciences. The ENABLEH2 project investigates critical technologies for cryogenic H2 applications in commercial aviation, including new combustion and heat management systems. This paper revolves around the design and construction of a core cooling flow facility which was commissioned to study and verify the potential benefits of incorporating a heat management system into the intermediate compressor duct (ICD).

The test facility is designed to operate continuously at rotor midspan chord Reynolds number up to 600,000 to allow for detailed aerothermal studies at a technical readiness level four. The two-stage axial compressor is representative of the low-pressure compressor and ICD of a mid-size commercial jet engine. The compressor is powered by a 147kW electric motor at 1920 RPM. The mass-flow and pressure ratio are controlled by restricting valves located at the inlet of the facility. A compact volute settling chamber, with an integrated thermal control system is used to control the inlet temperature and remove flow non-uniformities downstream the restrictor valves before entering the compressor. At the compressor inlet, a turbulence mesh is mounted to increase the turbulence intensity levels to 3-4% at the leading edge of the variable inlet guide vanes.

The compressor is mounted vertically to allow for easy access to the downstream ICD and mitigate non-axisymmetric mechanical loads. The compressor unit allows for optical and traverse access at two $\pm$ 9-degree sectors for all the rotor-stator interfaces. Upstream the OGV, there are four independent $\pm$ 180-degree access traverse systems. In the ICD, measurements are carried out by a single ABB robot with a U-shaped probe mount, providing full volume probing access of the ICD. At the first design iteration the ICD is designed to be instrumented with multi-hole probes, hot-wire anemometry and heat transfer measurement using IR-thermography.

The paper describes the facility and the process of achieving a high case similarity (engine representative) while maximising the quality of the experimental data over a large test domain, targets that often produce conflicting design demands.

KEYWORDS

Experimental, Low-pressure Compressor, ICD, Aerothermal, Cryogenic

NOMENCLATURE

A - Area (m^2)
B - Investigated Boundary (-)
c - Chord (m)
g - Pitch (m)
h_i - Channel Height (m)
K - Kelvin (K)
L - ICD Length (m)
Π - Pressure Ratio (-)
p - Pressure (Pa)
p_0 - Room relative Total Pressure (Pa)
$r_{1/2}$ - Rotor 1 or 2
R - Radial transport distance ICD (m)
Re - Reynolds Number (-)
$Re_{crit,L}$ - Critical Chord Reynolds Number (-)
$s_{1/2}$ - stator 1 or 2
T - Temperature (K)
$T_u = V'/V$ - Turbulence (%)
x - Arbitrary variable
$\dot{q}''_{air}$ - Convective Heat Flux
HEX - Heat Exchanger
HPC - High-Pressure Compressor
HS - Heat Management and Settling Chamber
ICD - Intermediate Compressor Duct
HS - Heat Management and Settling Chamber
LH_2 - Liquid Hydrogen
LPC - Low Pressure Compressor
OGV - Outlet Guide Vanes
R - Reading from device
RANS - Reynolds Average Navier Stokes
RMS - Root Mean Square
RTD - Resistance Temperature Detector
SFC - Specific Fuel Consumption (-)
$\dot{m}$ - Mass flow (kg/s)
σ - RMS of non-uniformity from average
γ - Specific Heat Ratio (-)
η_c - Isentropic efficiency (-)
$\bar{x}$ - Average of arbitrary variable

Introduction

Green liquid hydrogen (LH_2) is arguably one of the very few fuel candidates to enable carbon-neutral long-range commercial aviation. Liquid hydrogen has many distinct differences to classical Jet-A that from a propulsion unit design perspective adds complexity, but also offers many opportunities. One of the distinct difference and opportunity is the high heat capacity together with the low storage temperature of 22 K of LH_2 which enables the fuel to absorb large quantities of energy before entering the combustor. At a relatively high fuel injection temperature of 1000K, the heating capacity equals 10% of the lower heating value (140MJ/Kg) of the fuel. Instead of using fuel to perform this heating, the fuel can be pre-heated by strategically placed heat exchangers throughout the propulsive system. One of these locations is an intercooler in the compression process. Earlier presented intercooler turbofan concepts Zhao et al. [2015] showed a 4-5% decrease in specific fuel consumption(SFC). These concepts reject heat from the core flow into the bypass air and benefit mainly from a higher overall pressure ratio and reduced compression work. The cryogenic temperatures and high heat capacity of hydrogen allow for more power compact heat exchangers with less weight penalty and higher specific heat transfer rate. The fact the heat is injected into the fuel further increases the cycle efficiency compared to rejecting the heat to the free-stream air.

The ICD transports the core flow from the low-pressure compressor (LPC) to the high-pressure compressor (HPC) through an s-duct also known as a swan duct. From a system perspective, the duct length L should preferably be as short as possible to save weight but is aerodynamically constrained by the radial transport distance, ΔR, from the LPC to the HPC. Too aggressive a design, i.e. high $\Delta R/L$, would cause large radial pressure gradients and flow separation. Experimental investigations of this limitation are a relatively active topic with seve-

ral active high- and low-speed test facilities for aerodynamic investigation of the ICD such as Walker et al. [2013], Wallin et al. [2013]. An installation of an intercooler in the ICD would most likely require an increased wetted surface to cope with the expected heat transfer rate. This increased area can synergistically be used for heat transfer and to guide the flow radially, enabling a more compact and aggressive ICD.

An early numerical attempt at this design is presented in Jonsson et al. [2020a]. The design of this component is outside typical design parameters in turbomachinery. Hence, the numerical simulations require verification which is the facility's primal aim. A fully annular low-speed test facility with high dimensionless geometrical and aerodynamically similitude provide a good compromise between measurement quality and cost compared to the high-speed counterpart. Except for compressible effects, such a facility can reproduce many complex flow features present during full-scale operation that are challenging to numerically predict. Since there are no shocks present in the ICD and OGV a low-speed facility was found to be a suitable starting point. To the authors' best knowledge no facilities are aiming at studying the aerothermal performance of the ICD.

This work surrounds two intertwined targets of producing engine representative condition in a low-speed facility and maximise measurement quality. The work is divided into two but was achieved through an iterative process. The first part focuses on fundamental and practical aspects when designing the low-speed facility for engine representative conditions. The second part assesses performance evaluation methods and instrumentation in regards to the expected measurement uncertainty.

The Facility

General Features

The large-scale low-speed test facility is designed to accommodate operating conditions representative of future large-size geared commercial turbofan engines. Figure 1 illustrates the schematics of the facility and Table 1 includes the compressor and intermediate compressor duct design parameters. The test facility is semi-closed with an ambient static pressure recovery at the outlet of the ICD. Operational conditions are achieved by restricting the flow upstream and by regulating the input power to the compressor which drives the main flow through the facility. The flow is conditioned for thermal and pressure uniformity in a combined volute and flow conditioner, between the restrictor and the compressor inlet. The ICD is mounted downstream of the two-stage compressor and the ICD outlet is the outlet of the facility. The flow is recirculated into the facility for thermal stability, and to limit particle and noise mitigation.

Compressor design parameters

The 2.5 low-speed axial compressor is designed to accurately replicate the final stages of a modern high-speed LPC in the virtual engine VINK, Lejon et al. [2017]. The components in the compressor following the flow directions are: adjustable inlet guide vanes (IGV); first rotor (r1); a stator row (s1); second rotor (r2); and finally the outlet guide vane (OGV). The overall facility design was done at Chalmers in close collaboration with GKN Aerospace Sweden for the compressor unit. Note that the facility is designed for experimental purposes and does not represent any GKN Aerospace product characteristics. Below are some of the overall considerations and selections necessary before the design of the compressor could be initialised.

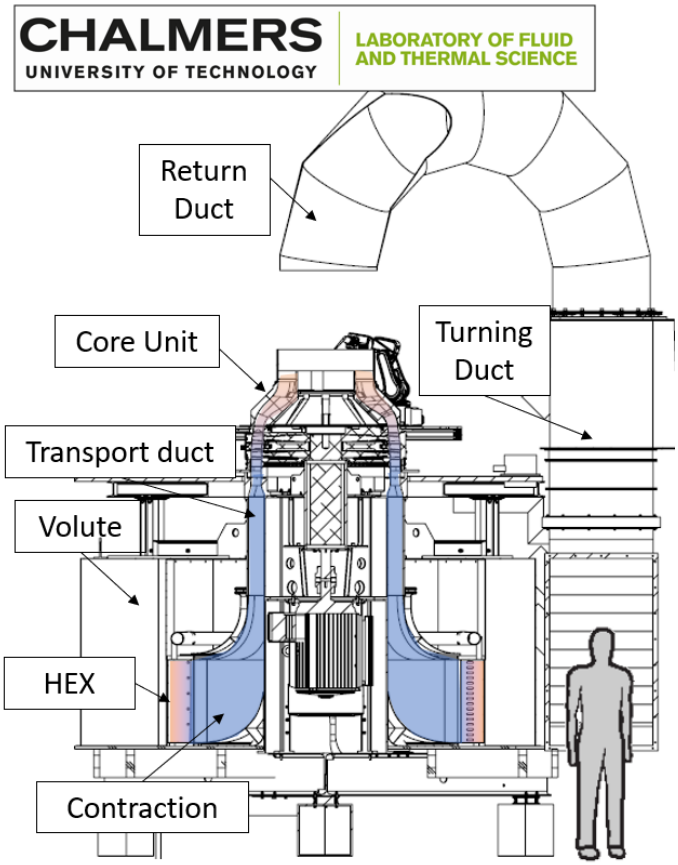

Figur 1: **Schematic view of the LPC test facility**

Rotational Speed ..	1920 rpm
Mass flow	17 kg/s
Pressure ratio	1.07
Temperature ratio ..	1.02
Tip Speed	100m/s
Axial Velocity	70m/s
Rotor $\mathrm{Re_c}$	6×10^5
Avg. Tip radius	620mm
Avg. Hub radius ...	540mm
Nr. stator Blades ...	75,124,126
Nr. rotor Blades ...	61,69
Avg. Aspect Ratio .	2.157
Avg. Tip Clearance	0.75mm

Intermediate Compressor Duct	
h_i	0.105
L	0.290
A_i/A_o	1.0
$\Delta R/L$	0.6

Tabell 1: **LPC and ICD Design Parameters**

Reynolds Number

Typical midspan chord rotor Reynolds number for an LPC in a large-sized commercial aviation engine is $\mathrm{Re} = 10^6$, this is beyond what practically could be reproduced in the laboratory. There is a general agreement of the existence of three operational regions for compressors, first the laminar region where a laminar separation occurs on the suction side, causing a rapid loss in performance and turning ability. Schaffler [1980] defined this region for a $\mathrm{Re}_{crit,L} < 10^5$, Wassell [1968] at $\mathrm{Re}_{crit,L} = 10^5$ and Carter Carter et al. [1957] $\mathrm{Re}_{crit,L} < 5 \times 10^4$. At a high Reynolds number, the polytropic efficiency becomes Reynolds number independent as surface features on the blades penetrates the viscous sublayer. This region is called the roughness region and is defined above $\mathrm{Re} = 6 \times 10^5$ by Carter in Schaffler [1980]. Between these two regions, the polytropic efficiency follows the function $k\mathrm{Re}^n$ where k and n differs between different correlations. The vast majority of low-speed test rigs operate in this region. To mitigate the risk of laminar separation a minimum Reynolds number was set to $2 - 3 \times 10^5$. To provide testing of 50% part load the design target of the facility was set to 6×10^5.

Turbulence intensity

The turbulence varies substantially in the gas-path of a compressor, with values in an order of magnitude higher in the hub and shroud boundary layers relative to midspan, Camp and Shin [1995]. Even though a single representative value cannot be defined, a turbulence level can be selected that mitigates the risk of non-representative flow feature that can occur in low-speed

facilities, such as natural laminar-turbulent transition along with the stator blades at lower Reynolds number. According to Mayle [1991], by-pass laminar-turbulent transition is greatly favoured at a turbulence level above 3%. Increasing the turbulence also mitigates the non-uniformity in the flow entering the compressor due to the high-pressure drop over the turbulence generators. Hence, at the inlet of the IGV, a minimum turbulence of 3-4% is selected and generated by turbulence screens with a canter gap width of 3.15mm and wire diameter of 1mm, following the guidelines in Groth and Johansson [1988].

Tip-clearance

Tip-clearance primarily affects the secondary flow structures, either by leakage through the tip clearance or by the scraping of the low momentum boundary layer at the shroud Denton [1993]. A smaller tip clearance will reduce the leakage but increase the scraping of the boundary layer. Sakulkaew et al. [2013] showed that for transonic compressors, there should be a theoretical minimum losses between the competing loss mechanisms at a tip clearance height of $0.1 - 1\%$ ε of the channel height h. Below a span-wise clearance of 0.4 %, Sakulkaew et al. [2013], Ell [2014] computed similar stage performance with and without tip-clearance. The tip-clearance effects on stall margin are often evaluated by the pitch-line gap g to tip clearance where values below 0.01 do not affect the stall margin. To allow features both caused by leakage flow and scraping, a tip clearance of 1%, $\approx$ 0.75 mm or $\varepsilon/g = 0.022$ is selected as the baseline for the compressor. The tip clearance can be varied by in-situ adjustment or by replacement of shroud inserts made of Ureol®. The relatively large tip clearance of 1% of h also reduces manufacturing costs on rotor and shroud as a larger throw is acceptable. A sensitivity analysis using the correlations from Koch [1981] and Denton [1993] provide performance variations in the order of $0.5 - 1\%$ for a throw of $\pm$ 0.075 mm.

Compressor stacking and design

With the identified fundamental targets the stacking and blading of the compressor were initialised. This process was performed in close collaboration between the experimental and aerodynamic designer, starting with fundamental one-dimensional design correlations until the three-dimensional stacking. The intricate design process of the compressor is beyond the scope of this work but fundamental compromises are still of interest. From an instrumentation perspective, and for manufacturing and access to test geometries the facility should be large and slow rotating. The large scale and slow rotation allows for a high ratio of sampling rate to physical phenomena frequency, further simplifying instrumentation. However, with relatively limited power, the aerodynamic designer prefers a smaller faster spinning unit as this allows for higher engine similitude in terms of compressibility. Hence, the majority of discussions between the experimentalist and the aerodynamic designer centre around channel height h and RPM. Some adjustment on rotor and stator blades thickness from high speed to low speed as described by Wisler [1985] was a performance to mitigate natural frequency interaction of rotor blades, to ease manufacturing demands on the leading edge, and to allow for pressure tap installation. The final design in terms of blade loading, flow coefficient, hub-to-tip ratio, diffusion ratio and blade aspect ratio were within 5% from the targeted compressor VINKs two final LPC stages. The largest difference between them was the pressure ratio as with similar stage loading but slower rotation the pressure ratio will be lower. The compressor multi-stage performance, including the IGV and ICD, was evaluated numerically using Ansys™ CFX, with the RANS $k - \omega$ SST turbulence model, mixing-plane for the interfaces and enhanced wall functions to approximate

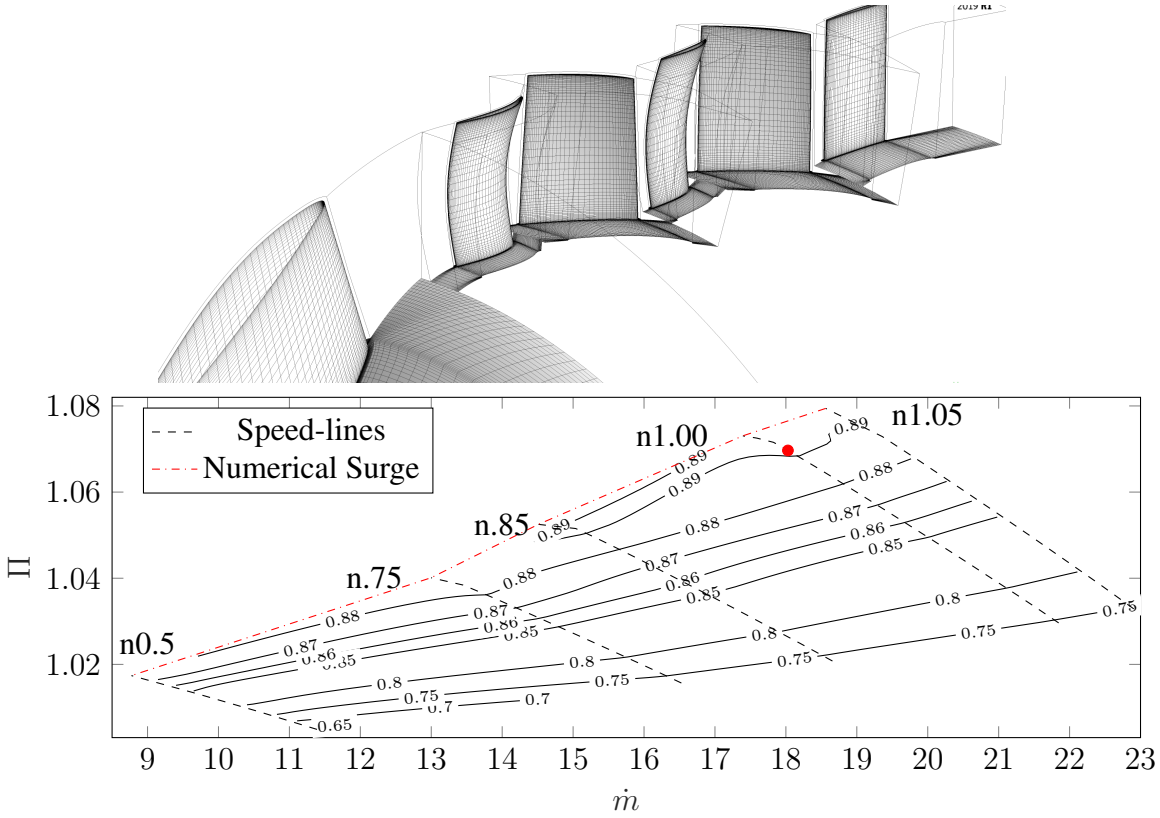

Figur 2: **Mesh distribution of the numerical domain for the compressor (top) with the performance maps from numerical results (below). The thick black lines show corrected speed-lines, the dashed red line represents the stall limit, contours show isentropic efficiency. The design point is marked with a red marker**

the flow in the wall region. Each stage has around 450,000 elements based on a mesh sensitivity of a high-speed case in Lejon et al. [2017]. Performance variation for a constant rotational speed is achieved by varying the inlet stagnation pressure. An inlet turbulence level of 5% is specified at the inlet, and at the outlet, a constant value of static pressure is specified. At the design point, y-plus ranges between 30-40 along the blade surfaces. Five different corrected speed lines are evaluated, 0.5, 0.75, 0.85, 1 and 1.05. These are grouped in the compressor map shown in Fig. 2 as black lines with a marking for each preformed simulation. The pressure ratio PR is shown on the y-axis and corrected mass flow $\dot{m}$ along the x-axis. The isentropic efficiency is illustrated by contours and the numerical surge line is shown as a numerical red dashed line. The numerical dashed lines are defined as the point when the stability of the simulations was compromised and independent of iteration no stable solution was found.

Inlet flow conditions

Axial compressors are relatively sensitive to changes in blade flow angles and hence also inlet flow distortions, local inlet distortions are measurable through several stages Longley [1990] but does in general stay local. Large scale non-uniformity can instead be challenging to accommodate as the compressor operation will vary with tangential location and cause an early stall or other unexpected scenarios. Therefore, local variation was accepted but not large scale tangential variations. To provide such inflow to the LPC, a compact integrated heat management and

settling chamber (IHS) was designed. The IHS consists of a constant azimuthal velocity volute, centre mounted radial shim heat exchangers, a contraction and a transport duct which are marked out in Fig. 3. Aerodynamically, the shims in the heat exchangers act as guide vanes and flow conditioners as they both reduce axial and azimuthal momentum in the flow. In the downstream contraction, the flow is accelerated to the transport duct which also contains a slight contraction before the fore-mentioned turbulence screens.

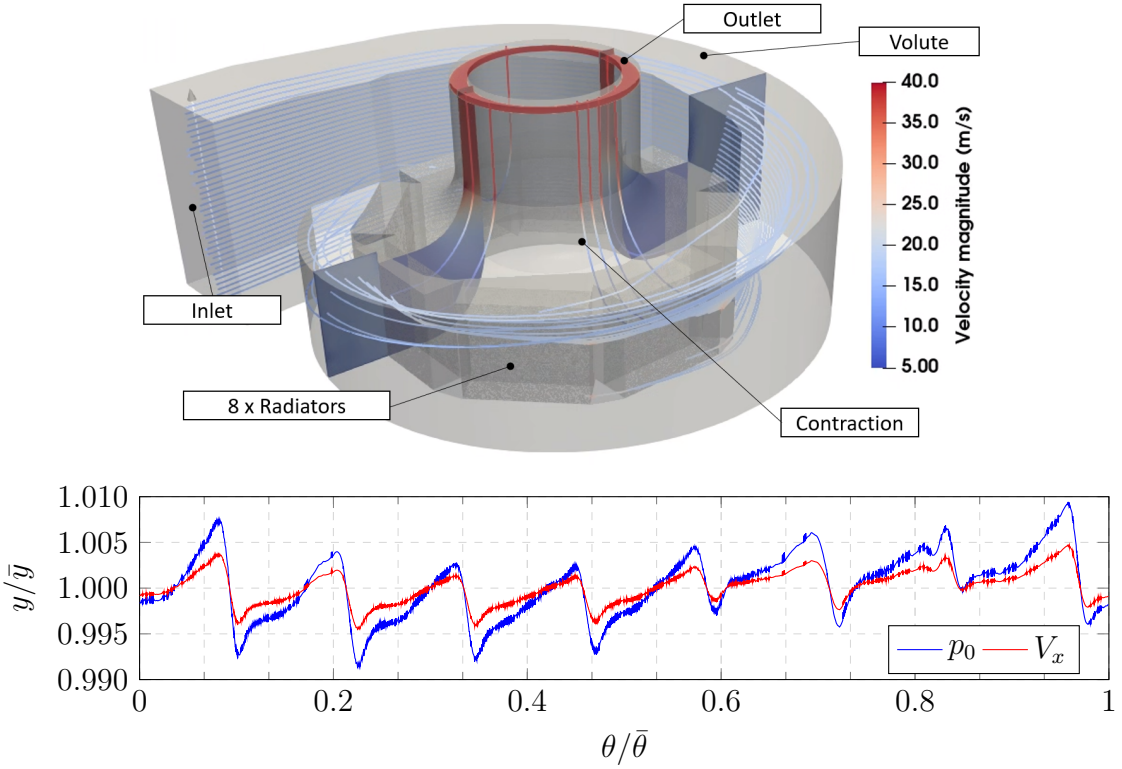

Figur 3: **Midspan Velocity and pressure distribution 300mm downstream the contraction outlet (Upper) and the streamlines from the numerical simulation (Lower). The minor grid represent tangential resolution for inlet condition probe access**

The design of the IHS was evaluated using STAR-CCM+^{TM} using RANS and realizable $k-\epsilon$ two-layer turbulence model with an all-y+ treatment in a steady state simulation with constant density air. The choice for this simulation setup was motivated by the low velocity gradients, low temperature gradients and no compressibility effects expected in the IHS. A polyhedral and prism layer mesher were used to mesh the computational domain and the near-wall regions respectively. The wall y+ was maintained above 30 to enable the use of wall functions. The turbulence was specified by an intensity of 6% and a length scale of half the distance between resistor baffles (0.1m). The internal geometry of the heat exchangers was not incorporated into the simulation, instead, the radiators were modelled using the porous region approach in STAR-CCM+^{TM}. The increase in velocity and a pressure drop when the flow passes through the porous region changes were modelled using the porosity, tortuosity, porous inertial resistance and porous viscous resistance. The porosity and the tortuosity were set to 0.6 and 1 respectively. The porous inertial resistance and porous viscous resistance were implemented by the means of an orthotropic tensor and were set to 30kg/m4 and 135.5 kg/m3-sec respectively in the direction perpendicular to the radiator inlets and infinity in other directions. The porous region coeffi-

cients were tuned to adhere to manufacturer specifications to yield a pressure drop of 300Pa for an axial inlet flow of 5.1m/sec. The contraction was first evaluated with an axisymmetrical simulation where the duct was optimised for uniform outlet profile and was later integrated with the full simulation. The volute and contraction performance was evaluated using total pressure and axial velocity 300 mm downstream of the contraction by the area-weighted RMS of flow variation from the mean flow properties σ as in Steen et al. [2014] which is defined in Eq. 1. A mesh independence study starting with a 3.2 million cell-sized mesh showed that a variation in outlet total pressure and velocity below 0.1% could be achieved with a mesh between 5.2 and 7.7 million cells.

$$\sigma = \sqrt{\frac{\sum_{i=1}^{n} A_i (x_i - \bar{x})^2}{\sum_{i=1}^{n} A_i \bar{x}^2}} \qquad x = V, p_0 \tag{1}$$

The computed radial non-uniformity σ, including the boundary layer, is in the order of $1 - 3\%$. If data points in the boundary layer are neglected the variations are below 1% for both velocity and pressure variations. The normalised total pressure and velocity at midspan and 300mm downstream of the contraction are shown in Fig. 3. To accurately capture inlet conditions, fifteen radial evaluation access points are available upstream of the IGV which locations are illustrated as minor grid lines in Fig. 3.

Instrumentation approach

The evaluation of instrumentation configurations is performed in the flow field from the beforementioned numerical simulations. This way transducers and probes can early be evaluated in different configurations before the facility is inaugurated. For this facility, the performance is primarily evaluated by gas path studies, i.e. gas property changes between boundaries. This method is thermodynamically simple but is complex to perform with high confidence. This complexity can primarily be derived from the challenge to capture the true average of the investigated boundary. However, before assessing the uncertainty of a mean from many data points, the single point acquisition uncertainty needs to be assessed, which is performed in this section. More conventional evaluation methods such as shaft input power (through strain gauges), system thermal balance (cooling flow), and static rakes are installed but primarily for monitoring purposes and are not further discussed. There are three primal boundaries of interest, shown in Fig.4, the inlet of the compressor B_A, the interface between the compressor and ICD called B_B and finally the outlet of the ICD B_C. The focus of the investigation is the performance of components in the ICD and hence the instrumentation has been designed with the focus at and in between the boundary B_B and B_C. For heat transfer studies with the original aero surfaces or integrated heat exchanger with low solidity, the differential gas temperature changes will be too small to measure, instead, IR-thermography will be used to deduce the local heat transfer rate as in Jonsson et al. [2020b]. The facility is designed so that the majority of studies in the ICD, integrated heat exchanger and compressor share the same approach, instrumentation and post-processing.

Traverse details and Special Instrumentation

All traverse systems share the same mounting mechanism so the probes can be mounted at all locations. Thirty-two access points for static sensors and radial traversing are located around the compressor unit. Fifteen of these are mounted upstream the IGV to capture the inlet conditions

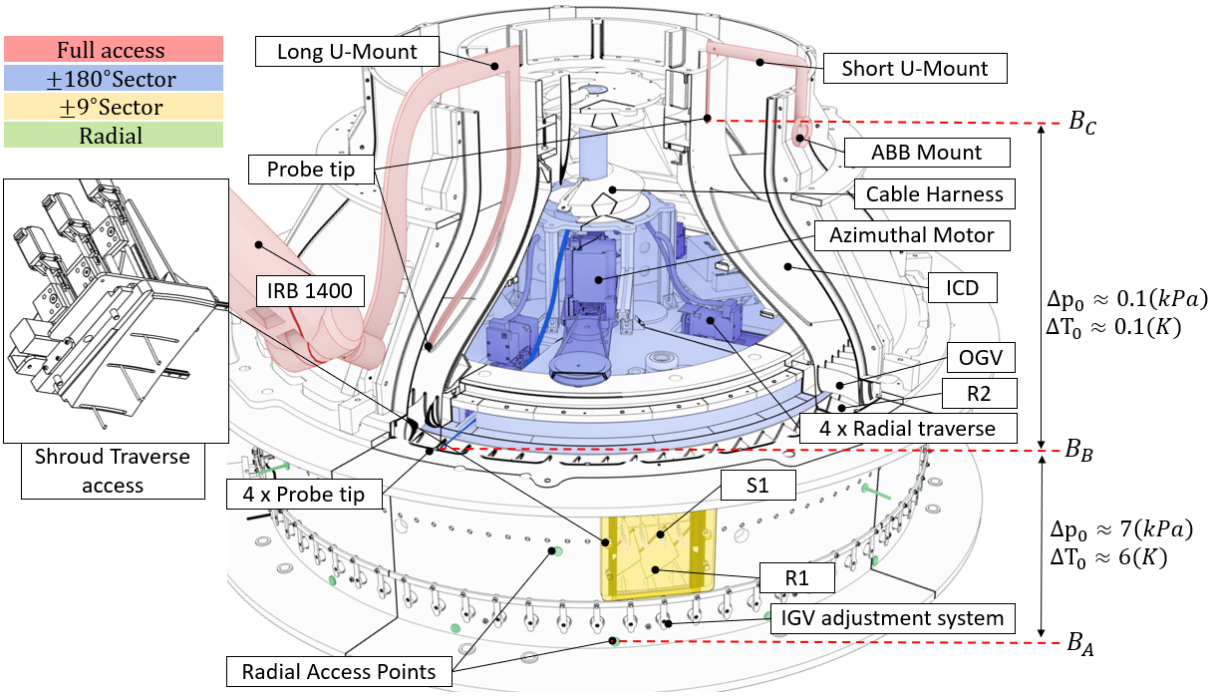

Figur 4: **Section cut of the ICD mounted on top of the compressor unit with part descriptions and colour scheme depending on access type. Boundary layer index positions are illustrated together with expected differential values of total pressure and temperature at design conditions**

at B_A. Figure 4 shows a section-cut of the ICD when mounted on top of the compressor unit. The green shaded region show radial traverse access, the yellow shaded regions show access where a sector of $\pm 9°$ traversing is possible through a window in the shroud and the blue shaded regions shows parts that can move $\pm 180°$ in the azimuthal drection. The shroud traverse system is shown to the left in Fig.4. At the inlet of the OGV, the $\pm 180°$ traverse system consists of four independent radial traverses is installed and are shown as dark blue in Fig. 4.

In the ICD, full volume traverse access is provided by an ABB IRB 1400 arm with a U-probe accessing through the outlet of the ICD. The position accuracy of an ABB robot is inversely proportional to the distance to the mounting point, the U-mount allows for more versatile traverse access and position accuracy without the need to penetrate the shroud. Both a short and long U-mount is shown in Fig.4, where the short is used for outlet studies and the longer for intermediate points, both probe tips have a similar length to the robotic arm mounting point of around 140mm. The ICD has been designed as two modules. All aero surfaces downstream the OGV can be lifted off with the traverse, OGV and all probe sill mounted. The parts downstream of the OGV are modular and relatively simple and cost-effective to replace. Shroud, hub and ICDs can be replaced with instrumented geometries with pressure taps as in Jonsson et al. [2018] or for heat transfer studies and local transition detection as in Jonsson et al. [2020b] and Jonsson et al. [2020c].

Transducers, probes and Uncertainties

As a first step, the boundary average, min and max values are used to select the smallest possible transducer range to mitigate unnecessary introduce sensors bias and increase sensitivity. For

this facility, this is achieved by the differential measurement between boundaries, B_A - B_B for compressor performance and B_B - B_C ICD investigations. These differential measurements are later related to a common reference such a room pressure and temperature. With ranges known, the expected accuracy for the single point measurement can be estimated from accreditation protocol and the impact of these on key performance indicator is evaluated by error propagation using the Talyor series approach. The key performance indicator and how these are experimentally evaluated for the LPC and ICD is shown in the first column of Table 2. Table 2 is also the baseline configuration shown with devices, expected measurement interval and accuracy. To mitigate probe-specific effects, both total pressure p_0 and temperature T_0 are measured differentially between two identical 1.6mm diameter Kiel probes. A micro manometer FCO-560 is used for pressure measurement. Total temperature is measured using resistance temperature detectors (RTD) from Pentronic AB, accredited to the uncertainty of 0.02K following International Electrotechnical Commission [2008].

Tabell 2: Table of the performance indicators together with connected devices, device accuracy and total uncertainty from Taylor expansion for typical measurement at design conditions

Performance Indicator	Device	Device Uncertainty	Total Uncertainty	Comment
$\Pi = \frac{p_{0_B}}{p_{0_A}}$	FCO-560	0.014%R	$\approx 0.02\%$	Identical 1.6 mm Kiel probes at B_A and B_B.
$\eta_c = \frac{(p_{0_B}/p_{0_A})^{\gamma/(\gamma-1)}-1}{(T_{0_A}-T_{0_B})/T_{0_A}}$	FCO-560 RTD	0.014%R 0.02K	$\approx 0.5\%$	P_t and T_0 are referenced to ambient at B_A
$P_{loss} = 1 - p_{0_C}/p_{0_B}$	FCO-432	0.25%R	$\approx 0.3\%$	Low solidity intercooler
$h = q''_{air}/(T_{surf} - T_{air})$	Primarily IR-Camera	0.75 K	3-8%	Local heat transfer, see Jonsson et al. [2020b].

Moreover, velocity and flow angles are measured using a 3mm diameter multi-hole at similar conditions probe as in Jonsson et al. [2018] and the same estimated uncertainties are assumed. For multi-hole probe measurements, a PSI-9116 and ESPDTC-32 is used. Mass-flow is measured by the pressure difference in the contraction between the transport duct and turbulence screens. The contraction discharge coefficient the contraction was calibrated with a standard 600mm diameter venturi meter [ASME International, 2004]. Hot wire anemometry is performed using a Dantec CTA 56C17 anemometry device and a NI-4461 DAQ for turbulence levels and time-resolved velocity measures.

Conclusion

This work presents the fundamental design choices and rationale in the design of the new low-speed compressor facility built to evaluate novel intermediate compressor duct heat exchanger solution for cryogenic fuelled aviation. Steady-state RANS simulations have been utilised to design and evaluate the 2.5-stage compressor performance and the upstream compact flow conditioner. The numerical results show that compressor key target was reached and as well as satisfactory inlet flow conditions with a non-uniformity σ of $1 - 3\%$ in total pressure and axial

velocity. The work describes the rationale behind the selection of instrumentation and individual sample point uncertainty has been estimated using Taylor Series expansion. The uncertainty of the key performance indicator for a compressor facility, namely, total pressure, isentropic efficiency has been assessed and is expected to be less than 1% except for an unknown bias offset in the mass-flow.

ACKNOWLEDGEMENTS

The authors would like to acknowledge the European Union for funding through the project ENABLEH2 in the H2020 programme, the Chalmers Laboratory of Fluids and Thermal Science for laboratory environment and equipment.

REFERENCES

Xin Zhao, Oskar Thulin, and Tomas Grönstedt. First and second law analysis of intercooled turbofan engine. *Journal of Engineering for Gas Turbines and Power*, 08 2015. doi: 10.1115/1.4031316.

AD Walker, AG Barker, JF Carrotte, JJ Bolger, and MJ Green. Integrated outlet guide vane design for an aggressive s-shaped compressor transition duct. *Journal of Turbomachinery*, 135(1), 2013.

Fredrik Wallin, Jörgen Olsson, Peter PJ Johansson, Euodia Krüger, and Martin Olausson. High speed testing and numerical validation of an aggressive intermediate compressor duct. In *Turbo Expo: Power for Land, Sea, and Air*, volume 55232, page V06BT38A003. American Society of Mechanical Engineers, 2013.

Isak Jonsson, Carlos Xisto, Hamidreza Abedi, Tomas Grönstedt, and Marcus Lejon. Feasability Study of a Radical Vane-Integrated Heat Exchanger for Turbofan Engine Applications. In *Proc. of ASME Turbo Expo 2020*, Turbo Expo: Power for Land, Sea, and Air, 09 2020a. doi: 10.1115/GT2020-15243.

Marcus Lejon, Tomas Grönstedt, Nenad Glodic, Paul Petrie-Repar, Magnus Genrup, and Alexander Mann. Multidisciplinary design of a three stage high speed booster. In *Turbo Expo: Power for Land, Sea, and Air*, volume 50794, page V02BT41A037. ASME, 2017.

A. Schaffler. Experimental and analytical investigation of the effects of reynolds number and blade surface roughness on multistage axial flow compressors. *Journal of Engineering for Power*, 102(1):5–12, 01 1980.

A. B. Wassell. Reynolds Number Effects in Axial Compressors. *Journal of Engineering for Power*, 90(2):149–156, 04 1968. ISSN 0022-0825. doi: 10.1115/1.3609154. URL `https://doi.org/10.1115/1.3609154`.

ADS Carter, GG Annear, GR Green, and CE Moss. *The effect of Reynolds number on the performance of a single-stage compressor*. Ministry of Aviation, Aeronautical Research Council, 1957.

T. R. Camp and H.-W. Shin. Turbulence Intensity and Length Scale Measurements in Multistage Compressors. *Journal of Turbomachinery*, 117(1):38–46, 01 1995. ISSN 0889-504X. doi: 10.1115/1.2835642. URL `https://doi.org/10.1115/1.2835642`.

Robert Edward Mayle. The 1991 IGTI Scholar Lecture: The Role of Laminar-Turbulent Transition in Gas Turbine Engines. *Journal of Turbomachinery*, 113(4):509–536, 10 1991. ISSN 0889-504X. doi: 10.1115/1.2929110.

Johan Groth and Arne V Johansson. Turbulence reduction by screens. *Journal of Fluid Mechanics*, 197:139–155, 1988.

J. D. Denton. The 1993 IGTI Scholar Lecture: Loss Mechanisms in Turbomachines. *Journal of Turbomachinery*, 115(4):621–656, 10 1993. ISSN 0889-504X. doi: 10.1115/1.2929299.

S Sakulkaew, CS Tan, E Donahoo, C Cornelius, and M Montgomery. Compressor efficiency variation with rotor tip gap from vanishing to large clearance. *Journal of turbomachinery*, 135(3), 2013.

Predictive Capability of CFD Models for Transonic Compressor Design, volume Volume 2B: Turbomachinery of *Turbo Expo: Power for Land, Sea, and Air*, 06 2014. doi: 10.1115/GT2014-27019.

C. C. Koch. Stalling Pressure Rise Capability of Axial Flow Compressor Stages. *Journal of Engineering for Power*, 103(4):645–656, 10 1981. ISSN 0022-0825. doi: 10.1115/1.3230787. URL `https://doi.org/10.1115/1.3230787`.

D. C. Wisler. Loss Reduction in Axial-Flow Compressors Through Low-Speed Model Testing. *Journal of Engineering for Gas Turbines and Power*, 107(2):354–363, 04 1985. ISSN 0742-4795. doi: 10.1115/1.3239730. URL `https://doi.org/10.1115/1.3239730`.

J. P. Longley. Measured and Predicted Effects of Inlet Distortion on Axial Compressors. volume Volume 1: Turbomachinery of *Turbo Expo: Power for Land, Sea, and Air*, 06 1990. doi: 10.1115/90-GT-214.

Laura-Cheri Steen, Judith Van Zante, Andy Broeren, and Mark Kubiak. Flow quality surveys in the settling chamber of the nasa glenn icing research tunnel (2011 tests). In *4th AIAA Atmospheric and Space Environments Conference*, page 2935, 2014.

Isak Jonsson, Valery Chernoray, and Radheesh Dhanasegaran. Infrared thermography investigation of heat transfer on outlet guide vanes in a turbine rear structure. *International Journal of Turbomachinery, Propulsion and Power*, 5(3):23, 2020b.

Isak Jonsson, Chernoray Valery, and Borja Rojo. Surface roughness impact on secondary flow and losses in a turbine exhaust casing. In *Proc. of ASME Turbo Expo 2018*, 2018.

Isak Jonsson, Srikanth Deshpande, Valery Chernoray, Oskar Thulin, and Jonas Larsson. Experimental and numerical study of laminar-turbulent transition on a low-pressure turbine outlet guide vane. In *Proc. of ASME Turbo Expo 2020*, 2020c.

IEC International Electrotechnical Commission. Iec60751. Technical report, International Electrotechnical Commission, 2008.

ASME ASME International. Flow measurement PTC 19.5. Technical report, ASME International ASME, 2004.